

## Fabrication of Piezoelectric Diaphragm using Lead Zirconate Titanate (PZT) Films

E. Hong<sup>1</sup>, S.V. Krishnaswamy<sup>1,2</sup>, C.B. Freidhoff<sup>2</sup> and S. Trolier-McKinstry<sup>1</sup>

<sup>1</sup>Materials Research Institute, The Pennsylvania State University, University Park, PA 16802

<sup>2</sup>Northrop Grumman Electronics Systems, Baltimore, MD 21203

### ABSTRACT

Piezoelectric diaphragms were fabricated using bulk micromachining. The diaphragms had a unimorph structure, where  $\text{Pb}(\text{Zr}_{0.52}\text{Ti}_{0.48})\text{O}_3$  (PZT) and thermally grown silicon oxide ( $\text{SiO}_2$ ) films were used as the active and passive layers, respectively. To actuate the diaphragms, two modes were designed:  $d_{31}$  and  $d_{33}$ -mode. For  $d_{31}$ -mode diaphragms, a Si wafer with Pt/Ti/ $\text{SiO}_2$  ( $0.5 \mu\text{m}$ ) was coated with  $\sim 1.2 \mu\text{m}$  PZT. A Cr/Au top electrode was then evaporated. Each layer including the bottom electrode was patterned into a circular shape. To fabricate  $d_{33}$ -mode diaphragms, a Si wafer with thermal  $\text{SiO}_2$  ( $0.5 \mu\text{m}$ ) was coated with  $\sim 0.3 \mu\text{m}$   $\text{ZrO}_2$  and  $\sim 1.6 \mu\text{m}$  of PZT. On top of these layers, a Cr/Au top electrode was deposited and patterned into a ring-shaped interdigitated transducer. Finally, both  $d_{31}$  and  $d_{33}$ -mode diaphragms were released using deep reactive ion etching. Diameters of the fabricated diaphragms were in the range of  $600 \mu\text{m}$  and  $1000 \mu\text{m}$ . For  $d_{31}$ -mode diaphragms, the dielectric constant and loss of the released piezoelectric layer at 1 kHz were  $> 800$  and  $< 2\%$ , respectively. The remanent polarization was  $\sim 20 \mu\text{C}/\text{cm}^2$  and the coercive field was  $\sim 61 \text{ kV}/\text{cm}$ . Ferroelectric measurements showed well-developed hysteresis loops for the  $d_{33}$ -mode diaphragms. Both  $d_{31}$  and  $d_{33}$ -mode diaphragms behave as membranes rather than plates. Their measured resonance frequencies were consistent with calculations from an analytic model for circular membranes and ANSYS finite element analysis.

### INTRODUCTION

Piezoelectric materials have been incorporated into many microelectromechanical systems (MEMS) to provide sensing and actuation functions [1]. To actuate cantilever, bridge and diaphragm structures, unimorphs, consisting of a piezoelectric layer and a passive layer, are usually adopted. In many cases, a  $d_{31}$ -mode has been used, where a piezoelectric layer is sandwiched between two metal electrodes. The piezoelectric film is then poled and driven through its thickness. The strain generated through the  $d_{31}$  coefficient results in flexure of the structure. In contrast,  $d_{33}$ -mode can be also considered. Here, a piezoelectric layer is poled parallel to the passive layer using an interdigitated transducer (IDT). When an electric field is applied to the IDT, the strain generated by  $d_{33}$  coefficients results in the bending of the structure. In many perovskite ferroelectric materials, the  $d_{33}$  constant is two times larger than  $d_{31}$ , and hence the interest in the  $d_{33}$ -mode in our study. Originally, this idea was proposed by Kugel et al. for bulk PZT actuators [2]. In addition, Xu et al. reported the sensing properties of PZT films deposited on silicon wafer using this mode [3]. Until now, there are few reports on  $d_{33}$ -mode actuated micromachined devices.

In this study, PZT was incorporated into a diaphragm structure.  $d_{31}$  and  $d_{33}$ -mode piezoelectric diaphragms were fabricated on 4" silicon wafers. The dielectric and ferroelectric properties of the piezoelectric layer of released structures were measured. To characterize the

actuation, the resonance frequencies were measured and compared with calculations from an analytic model and finite element analysis using ANSYS.

## EXPERIMENTAL PROCEDURE

Diaphragms were fabricated on 4" silicon wafers, with 0.5  $\mu\text{m}$  thermal oxide. This oxide will act as the passive layer in a unimorph. Figure 1 shows the process flows of  $d_{31}$  and  $d_{33}$ -mode diaphragms.

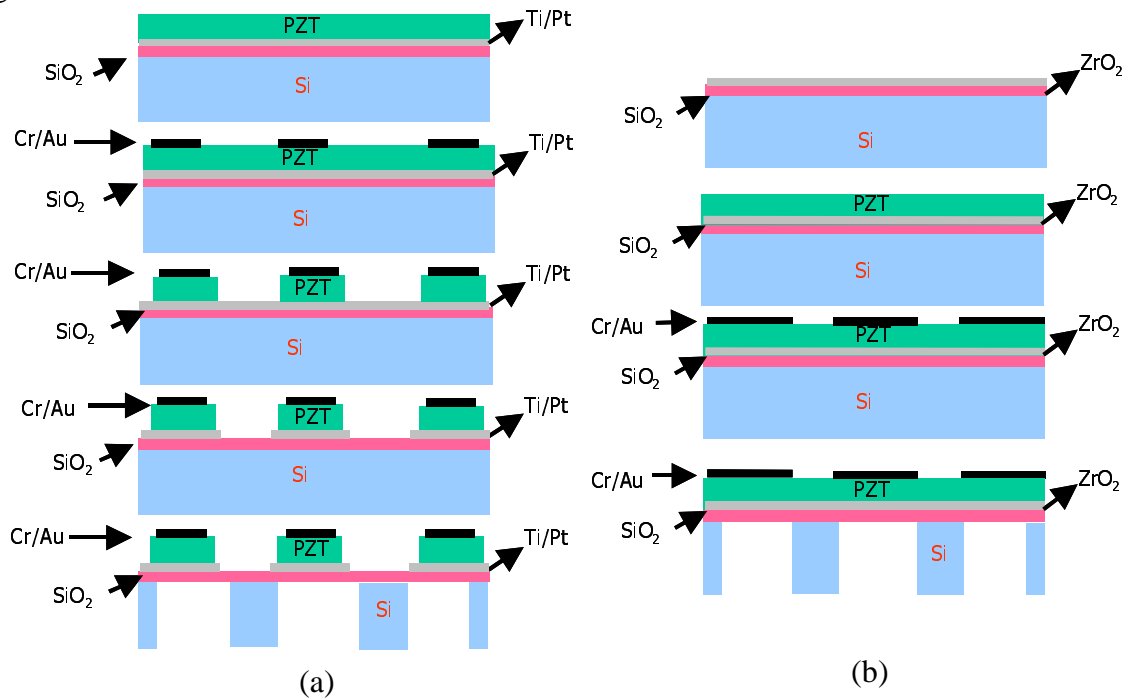


Figure 1. Process flows of (a)  $d_{31}$ -mode and (b)  $d_{33}$ -mode diaphragms.

In  $d_{31}$ -mode devices, Ti/Pt was deposited by sputtering for the bottom electrode. PZT was then deposited by a 2-methoxyethanol (2-MOE) based sol-gel method [4]. To deposit one layer of PZT, a 0.75 M PZT solution was spin-coated at 1500 rpm for 30 seconds using a photo-resist spinner. The layer was pyrolyzed at 450°C for 1 min and annealed at 700°C for 1 min using a rapid thermal annealer. To obtain the desired thickness, the spin-coating and thermal processing were repeated. Cr/Au was then deposited by e-beam evaporation. After all deposition processes were finished, each layer was patterned using standard photolithographic techniques. The Au layer was etched using a mixture of 42% KI: 3% I: 55% H<sub>2</sub>O (Transene Inc., Danvers MA). The Cr film was then etched using a mixture of 6% HNO<sub>3</sub>: 16% (NH<sub>4</sub>)<sub>2</sub>Ce(NO<sub>3</sub>)<sub>6</sub>: 78% H<sub>2</sub>O (Transene Inc., Danvers MA). The PZT film was etched by two-step etching process developed by Wang [5]. First, a 10:1 buffered oxide etcher (BOE, which is 10 NH<sub>4</sub>F: 1 HF) was used to remove the majority of the PZT. Second, a 2 HCl: 1 H<sub>2</sub>O solution for 30 seconds at 45°C was used to remove insoluble fluoride residue. The Pt/Ti layer was removed by reactive ion etching using a gas mixture of Ar (40sccm) and Cl<sub>2</sub> (10sccm) at 10 mTorr with a DC bias of 600V. Finally, diaphragms were released by deep reactive ion etching (DRIE). For  $d_{33}$ -mode devices, instead of a bottom electrode, a ZrO<sub>2</sub> layer was deposited on the SiO<sub>2</sub>/Si wafers by a 2-MOE

based sol-gel method. A 0.4 M  $\text{ZrO}_2$  solution was spin-coated at 3000 rpm for 30 seconds. The thermal treatment of the  $\text{ZrO}_2$  film was identical with those used for PZT. The  $\text{ZrO}_2$  layer was then annealed at  $700^\circ\text{C}$  for 3 hours using a furnace. The PZT layer was then deposited. Cr/Au was evaporated and patterned into interdigitated transducers (IDT). The IDTs were ring-shaped and the width of the IDT finger was  $7.5\ \mu\text{m}$ . The IDT spacing was 7.5, 10 or  $12.5\ \mu\text{m}$ . Again, the diaphragms were released using DRIE. Diameters of diaphragms in both modes were in the range of  $600\ \mu\text{m}$  and  $1000\ \mu\text{m}$ . The orientations and structures of the deposited PZT and  $\text{ZrO}_2$  layers were determined by x-ray diffraction technique (XRD) and scanning electron microscopy (SEM). To characterize the dielectric and ferroelectric properties of the PZT layer, dielectric and hysteresis measurements were conducted using a HP4192A LF impedance analyzer and a RT-66A Ferroelectric Test system (Radiant Technology, Inc). In addition, the mechanical resonances of diaphragms were characterized by a HP4194A impedance gain analyzer. These resonances frequencies were compared with calculations from an analytic model for circular membranes and an ANSYS finite element analysis (FEA).

## RESULTS AND DISCUSSION

### Structure and Crystallinity of Layers

PZT films deposited on Pt ( $d_{31}$ -mode devices) had (111) preferred orientation, suggesting that the PZT layer was templated by the Pt bottom electrode. However, the PZT film on  $\text{ZrO}_2$  ( $d_{33}$ -mode) was randomly oriented. This is reasonable because the PZT film was grown on a mainly amorphous  $\text{ZrO}_2$  layer. Cross-sectional views of both types show columnar growth of the PZT and  $\text{ZrO}_2$  films. The thicknesses of the PZT in the  $d_{31}$ -mode and  $d_{33}$ -mode diaphragms were  $\sim 1.2\ \mu\text{m}$  and  $\sim 1.6\ \mu\text{m}$ , respectively. The thicknesses of  $\text{ZrO}_2$  and  $\text{SiO}_2$  layers were  $\sim 0.3\ \mu\text{m}$  and  $\sim 0.5\ \mu\text{m}$ , respectively.

### Fabricated Diaphragms

Figure 2 shows the fabricated diaphragms. The layers were clearly etched. In  $d_{31}$ -mode diaphragms, the diameter of a diaphragm was similar to the diameter of the top electrode. In the  $d_{33}$ -mode diaphragm shown in Figure 2 (b), the diaphragm diameter was 40% bigger than the IDT diameter.

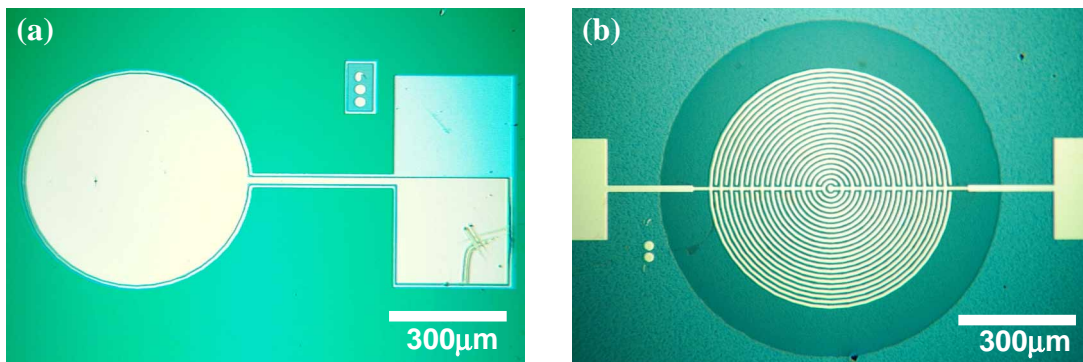


Figure 2. Optical pictures of (a)  $d_{31}$ -mode and (b)  $d_{33}$ -mode diaphragms.

Electrical Properties

The dielectric constant was 850 in  $d_{31}$  mode diaphragms. Dielectric losses in both modes were below 2%. The ferroelectric measurements of PZT layers in both modes exhibit well-developed hysteresis loops as shown in Figure 3. In  $d_{31}$ -mode diaphragms, the remanent polarization and coercive field were  $20 \mu\text{C}/\text{cm}^2$  and  $61 \text{ kV}/\text{cm}$ .

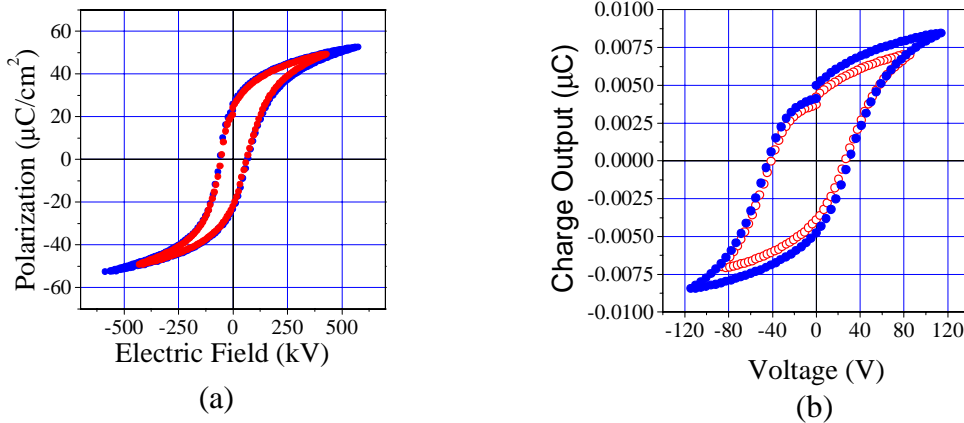


Figure 3. Hysteresis loops of (a)  $d_{31}$ -mode (diaphragm diameter:  $600 \mu\text{m}$ ) and (b)  $d_{33}$ -mode (IDT diameter:  $600 \mu\text{m}$ , IDT spacing:  $7.5 \mu\text{m}$ )

Mechanical Resonance

Three lowest resonance frequencies of  $d_{33}$ -mode diaphragms excited with applied ac electric fields are shown in Figure 4(a). Vibration of diaphragms can be expressed by plate or membrane theory [6]. The fabricated diaphragms followed membrane theory, which is expressed by the following equation.

$$f = \frac{\lambda}{2\pi r} \sqrt{\frac{T}{\rho h}} \dots\dots\dots (1)$$

where  $r$  is the radius of the diaphragm,  $T$  is the tension,  $\rho$  is the density,  $h$  is the thickness and  $\lambda$  is a constant depending on the vibration modes. As shown in Equation (1), the resonance frequencies of membranes are inversely proportional to the radius of the diaphragms as shown in Figure 4(b). Using a  $d_{33}$ -mode diaphragm (IDT diameter:  $700 \mu\text{m}$ , diaphragm diameter:  $980 \mu\text{m}$ ), the measured resonance frequencies were compared with calculations from Equation (1) and an ANSYS FEA.

To calculate the resonance frequencies of each vibration mode using Equation (1), the tension and density of the diaphragm were required. The average density of a diaphragm can be calculated by multiplying the density of each layer with its fraction of the thickness. Using the measured first resonance, the value of the tension on the diaphragm can be extracted [7]. From this value, the calculated stress was  $67 \text{ MPa}$ . The sequential resonance frequencies were then calculated using different  $\lambda$  values depending on the vibration modes. In an ANSYS FEA, a diaphragm was modeled using Shell 99 elements, which can model multilayers [8]. In a modeled diaphragm, the average stress of  $67 \text{ MPa}$  was induced through a static analysis. The modal analysis of the prestressed diaphragm was then performed. The solution in the modal analysis was obtained by a reduced method using a Householder-Bisection-Inverse iteration [8]. The material properties of each layer and the results are summarized in Table I

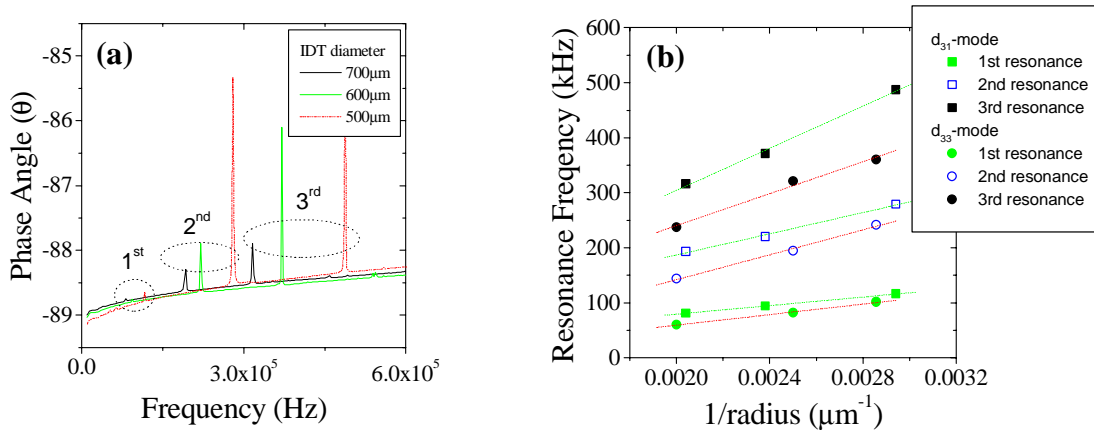


Figure 4. (a) Resonances from  $d_{33}$ -mode diaphragms and (b) three lowest resonance frequencies of  $d_{31}$  and  $d_{33}$ -mode diaphragms as a function of  $1/\text{radius}$ .

Table I. Material properties of each layer and resonance frequencies<sup>[9],[10],[11]</sup>

Layer	Density ( $\text{kg}/\text{m}^3$ )	Young's modulus (GPa)	Poisson's ratio
PZT	7600	101	0.3
ZrO <sub>2</sub>	5500	160	0.27
SiO <sub>2</sub>	2200	70	0.17

Mode (n,s)	(0,1)	(1,1)	(2,1)	(0,2)
Measured (kHz)	81	*	*	193
Analytic ( $\lambda$ ) (kHz)	81 (2.404)	129 (3.832)	173 (5.135)	186 (5.520)
FEA (kHz)	88	142	193	208

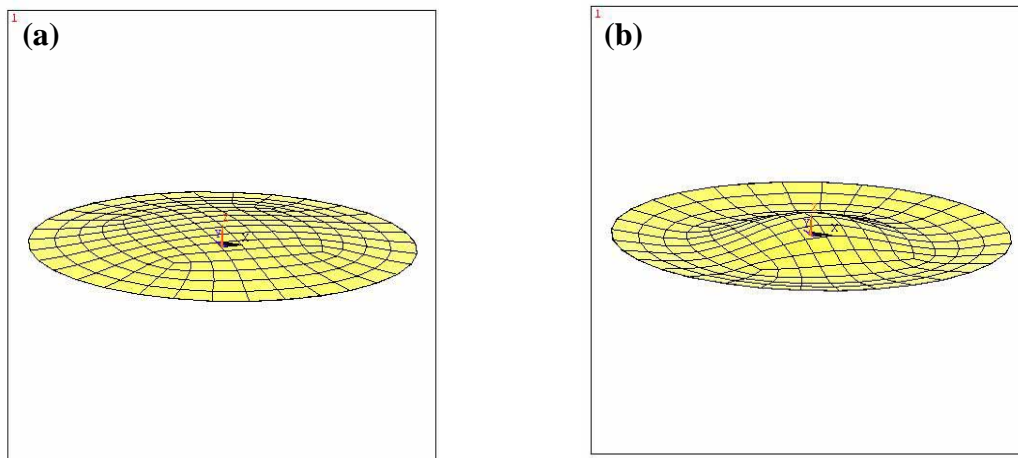


Figure 5. Modal shapes of (a) first mode (b) second mode of a  $d_{33}$ -mode diaphragm

From Table I, the two lowest resonances were symmetric modes. That is, asymmetric (1,1) and (2,1) modes were not excited. The results from the ANSYS FEA deviated from the measured values by 10%. One reason for this difference might be that the FEA treats the diaphragm as a multilayer stack but the analytic model only considers one layer. Therefore, the stress calculated from Equation (1) may give a higher value than the actual one. In addition, uncertainty in the material properties and assumed boundary conditions could also contribute to the deviation. Two of the predicted vibration modes from the FEA are shown in Figure 5 and were confirmed by a scanning vibrometer measurement.

## CONCLUSIONS

$d_{31}$  and  $d_{33}$ -mode diaphragms were successfully fabricated. In released structures, PZT films showed good dielectric and ferroelectric properties. The mechanical resonances of these diaphragms followed membrane theory. The measured results were consistent with calculations from an analytic model for circular membranes and ANSYS finite element analysis.

## ACKNOWLEDGEMENT

The authors would like to thank Dr. Furman for his advice in impedance measurements, Dr. Braggins for his help in designing the masks and Dr. Q. F. Zhou for helping prepare the  $ZrO_2$  solution. The research reported in this document was performed in connection with Cooperative Agreement number DAAD17-00-2-1001 with the U.S. Army Research Laboratory.

## REFERENCE

- [1] P. Muralt, J. Micromech. Microeng., **10**, 136-146 (2000).
- [2] V. D. Kugel et al., Appl. Phys. Lett., **69**, 2021-2023 (1996).
- [3] B. Xu et al., Appl. Phys. Lett., **75**, 4180-4182 (1999).
- [4] Q. F. Zhou et al., presented at the 2000 MRS Fall Meeting, Boston, MA, 2000.
- [5] L.-P. Wang, PhD. Thesis, The Pennsylvania State University, 2001.
- [6] W. Weaver et al., *Vibration Problems in Engineering*, 5th ed. (John Wiley and Sons, New York, 1990).
- [7] P. Muralt et al., Sensors and Actuators, **A 53**, 398-404 (1996).
- [8] ANSYS Release 5.6 User Manuals, 1999.
- [9] T. Tuchiya et al., J. Ceram. Soc. of Japan, **104**, 159-163 (1996).
- [10] L. Gan et al., Thin Solid Films, **290-291**, 362-366 (1996).
- [11] M. T. Kim, Thin Solid Films, **283**, 12-16 (1996).